JPE 13-3-6

http://dx.doi.org/10.6113/JPE.2013.13.3.381

A Sensorless PMDC Motor Speed Controller with a Logical Overcurrent Protection

M. G. Guerreiro*, D. Foito*, and A. Cordeiro†

*ESTSetubal, Polytechnic Institute of Setubal, Setubal, Portugal
†ISEL, Polytechnic Institute of Lisboa, Lisboa, Portugal

Abstract

A method to control the speed or the torque of a permanent-magnet direct current motor is presented. The rotor speed and the external torque estimation are simultaneously provided by appropriate observers. The sensorless control scheme is based on current measurement and switching states of power devices. The observers performances are dependent on the accurate machine parameters knowledge. Sliding mode control approach was adopted for drive control, providing the suitable switching states to the chopper power devices. Despite the predictable chattering, a convenient first order switching function was considered enough to define the sliding surface and to correspond with the desired control specifications and drive performance. The experimental implementation was supported on a single dsPIC and the controller includes a logic overcurrent protection.

Key words: PMDC motor, Sensorless speed control, Sliding mode control, Speed and torque observers

I. INTRODUCTION

In the last several decades a significant effort has been made to improve several aspects of the performance of electrical motors. The selection of the motor characteristics is made according to each particular application regarding different requirements, such as power supply available, operating conditions, efficiency, reliability and costs. Thanks to several advantages over DC motors, AC induction motors together with power electronics have found very wide field applications, especially where variable speed electrical drives are required. Nevertheless, traditional DC motors continues to provide solution to numerous applications in robotics, automotive, transportation, food, drug, chemical, paper and semiconductor industries [1]-[6]. It is also possible to find such motors in small appliances [7]-[9]. The use of DC motors satisfies most processes requirements in terms of accuracy and robustness of control due to the excellent torque-speed characteristic curve and easiness of speed control regardless the load torque.

Nowadays it is most usual to find DC motors operating in power ranges from very low to low (1 W-2 kW) [3], [9], [10] or else in power ranges from high to very high (150 kW-25 MW) [2], [11], leaving the mid power range mainly to AC induction motors.

Several control techniques have been designed to DC motors over the years, ranging from the classical control theory suited to control of linear processes, whose exact model is known, to control structures based on artificial intelligence (AI), such as fuzzy logic or artificial neural networks [12]-[17] where model parameters are not exactly known and subjected to variations during operation. Robust controllers based on adaptive and H∞ control techniques [3], [18]-[20] have also been proposed to overcome uncertainty conditions regarding the motor parameters and load conditions.

For many applications there is a continuous search for solutions to achieve speed or torque control without using mechanical sensors [6], [21]-[23]. Some of the reasons that motivate this search are due to reduction of costs, need for special arrangement for mounting and also reliability issues. However, this requires the design of new control techniques using speed and torque observers.

In this paper it is proposed a novel scheme for sensorless speed/torque control of permanent-magnet direct current motors (PMDC). The estimation of the speed/torque is carried out by extending the classical observer theory and the formulation is supported only on measurements of motor current and voltage or switching states of power devices.

Manuscript received Mar. 15, 2012; revised Mar. 12, 2013
Recommended for publication by Associate Editor Jung-Ik Ha.
†Corresponding Author: acordeiro@deea.isel.ipl.pt
Tel: +35-126-579-0000, Fax: +35-126-579-0043, Polytechnic Inst. of Lisboa
*ESTSetubal, Polytechnic Institute of Setubal, Portugal

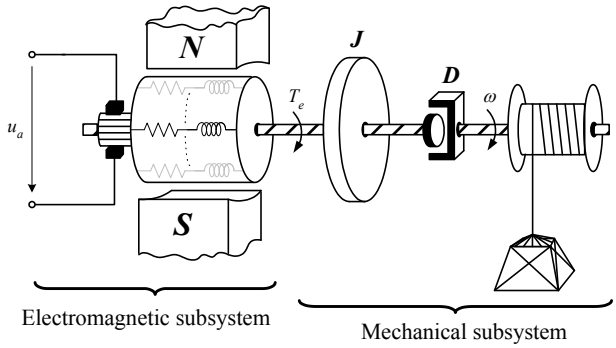

Fig. 1. Diagram of the electromagnetic and mechanical subsystems of a PMDC motor.

Although the estimation of speed and torque based on equations and parameters of PMDC motor are known, the simultaneously interconnection of such observers, as presented in this paper, do not seem explored. To ensure a certain level of robustness of the controller against to parameter variations and torque disturbances, a sliding mode (SMD) control strategy was adopted. Sliding mode control has been successfully applied to PMDC motor speed control [24], [25]. The switching control law such that the system trajectory can be trapped on the switching surface is based on a logical equation which brings simplicity and ease of implementation in digital signal processors.

In detail, this paper is organized as follows: in Section II the model of the PMDC motor is presented as well as the sliding mode control strategy. In Section III the current limiter is described providing the necessary overload protection. Section IV shows important aspects of observers design that will allow estimating the rotor speed and the load torque. Some simulations to observers performances under parameters variations are included. Section V is dedicated to succinct stability analysis. Section VI concerns about general hardware implementation. Section VII deals with experimental results and global drive performance. Finally, section VIII presents the conclusions of the developed work.

II. MOTOR SLIDING MODE CONTROL

A PMDC motor is constituted by an electromagnetic subsystem interconnected with a mechanical subsystem. The armature current resulting from the voltage applied interacts with the main flux and, as consequence, an electromagnetic torque is developed. This one is the input of the mechanical subsystem. The electromagnetic torque modifies continuously the rotor position imposing a certain angular speed, Fig. 1. The angular speed or the shaft torque is, according with the control objective, the usual mechanical subsystem output.

The mathematical model of the PDMC motor is based on the armature voltage equation and on the mechanical equation, according with (1).

$$\begin{bmatrix} \dot{i}_a \\ \dot{\omega} \end{bmatrix} = \begin{bmatrix} -r_a / L_a & -k_\phi / L_a \\ k_\phi / J & 0 \end{bmatrix} \cdot \begin{bmatrix} i_a \\ \omega \end{bmatrix} + \begin{bmatrix} 1/L_a & 0 \\ 0 & -1/J \end{bmatrix} \cdot \begin{bmatrix} u_a \\ T \end{bmatrix} \quad (1)$$

The state variables are the armature current i_a and the rotor speed ω. The armature voltage u_a is the control input or command action, and the torque T can be formally considered as a system input or, alternatively and more commonly, as a system disturbance. The torque T includes the load torque, the viscous and Coulomb friction, and all other unknown disturbances.

The motor parameters (the armature resistance r_a, the armature inductance L_a, the inertia moment of the rotor J, the torque constant k_ϕ) were considered as constant values.

The idea behind a control system consists of modifying its state according with some reference value. The tracking error vector, that is, the difference between the setpoint variable and the controlled variable, must be carried to zero. A simple and robust control method can be obtained using the variable structure system (VSS) theory. The state spatial domain of an n^{th} order system is an n-dimensional hyperspace where a convenient lower order sliding surface is defined to satisfy the control purpose. The general objective of the sliding mode control is to find the system state trajectory on to the specified surface along which the process can slide to its desired value. The process of sliding mode control can be divided into two stages. The first stage, known as the reaching stage, consists of assure that the initial error condition reaches the sliding surface in a finite time interval. In the second stage or sliding stage, a switching function guides the state trajectory on the sliding surface to nullify the tracking error.

If a system is described by a n^{th} order differential equation it can be used a sliding mode control with a $(n\text{-}1)^{th}$ order differential switching function [26] and so, if $n = 2$ the switching function $S(x,t)$ will simply have order one, according with (2). Where e_x is the tracking error of the state variable x and k_e is a tuning parameter used to define the sliding surface.

$$S(x,t) = \dot{e}_x + k_e e_x \quad (2)$$

Imposing $S = 0$ is equivalent to lead the state through a switching straight line to the origin of the phase plan $(e_x, \dot{e}_x)$. The initial objective was transferred; the actual objective became to nullify the switching function and, consequently, the error ex will tend exponentially to zero with a constant time $\tau_e = k_e^{-1}$. To achieve this purpose a discontinuous control action composed by the following switching law was chosen:

$$u = U \operatorname{sgn}(S) \quad (3)$$

Theoretically, with sufficiently high amplitude and frequency of the control action, the sliding mode control presents interesting properties such as robustness against modeling uncertainties, parameter variations and external

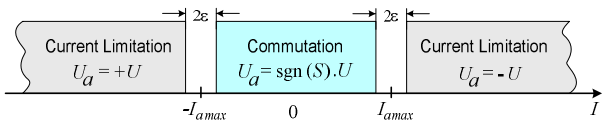

Fig. 2. Operation area of control algorithm with armature current limiter.

disturbances [27].

The switching law is directly responsible for decoding the discrete signals to apply to the four-quadrant chopper and, consequently, to the motor armature. This algorithm represents the basic structure of the PMDC motor control. Due to switching frequency limitations on certain power devices and the necessary time delays to prevent short circuits in the chopper branches, a serious and undesirable phenomenon called chattering is present. For low frequencies the chattering can be unacceptable. However, the high switching frequencies of modern semiconductors allow minimize, or even neglect this phenomenon.

III. Armature Current Limiter

The performance of the controller is the result of a control strategy whose main objective is to drive the system state to an equilibrium point according with the objectives.

As presented earlier (3), the sign of the switching function is fundamental in determining $+U$ or $-U$ armature voltages. Nevertheless, the system also needs to be protected against overload conditions. This additional function must be integrated within the control strategy and take precedence over the previous one for safety reasons.

An armature current limiter has been introduced to limit the effects of an eventual excessive motor heating and possible failures in other devices. Up to the permissible maximum current, the necessary voltage to be applied to the armature is only dependent on the primary control objective. However, if the current exceeds certain safety level, the control algorithm will tend to return the current to the maximum allowed value by applying the reverse voltage. A simple hysteretic comparator with limited bandwidth ε decides when the limiter should be used. Fig. 2 shows the safety operation area with sliding mode control between both current limitation regions.

The current limiter was implemented using a simple logic function (4), with logic variables. If the absolute value of armature current does not reach its maximum ($abs\_i_a = 0$) then the armature voltage sign (sgn_U_a) will be equal to the switching function sign (sgn_S or $sgn(S)$). Otherwise, the armature voltage sign will have opposite logic sign to the armature current sign (sgn_i_a) as way to reduce it.

$$\mathrm{sgn}\_Ua = \left(\mathrm{sgn}\_S \wedge \overline{abs\_i_a}\right) \vee \left(abs\_i_a \wedge \overline{\mathrm{sgn}\_i_a}\right) \quad (4)$$

The armature current limitation integrated in the switching law can be conceptually described by the diagram block of Fig. 3. This can be easily implemented with analog or digital devices such as dsPICs or FPGAs.

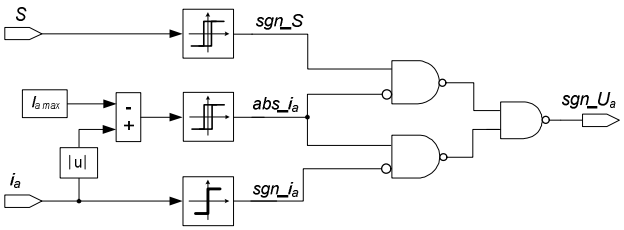

Fig. 3. Diagram block of the current limiter integration in the switching law.

TABLE I
Decision Table without Simultaneous Current and Speed Limiter

abs_i_a	abs_ω	sgn_U_a	Remark:
0	0	sgn_ S	Sliding mode control
0	1	$\overline{\mathrm{sgn}\_\omega}$	Speed limitation
1	0	$\overline{\mathrm{sgn}\_i_a}$	Current limitation
1	1	see table 2	see table 2

TABLE II
Decision Table with Simultaneous Current and Speed Limiter

sgn_i_a	sgn_ω	Sgn_U_a	Remark:
0	0	1	Current & speed increasing
0	1	STOP	Abnormal situation
1	0	STOP	Abnormal situation
1	1	0	Current & speed decreasing

When both current and speed signs are equals and exceed the absolute values all together, the limiter can counteract both quantities simultaneously (see table II) since this represents a typical motor operation. This requires reducing the average voltage applied to the armature. Nevertheless, if current and speed have different signs the limiter is not capable of adjust both quantities simultaneously. This means that the machine is operating as generator and the maximum braking current was exceeded. In practice this can be considered as an abnormal condition and the drive must stop since it is not feasible with the proposed solution increase and decrease the average voltage at the same time. Also, if possible, the shaft has to be blocked or the mechanical load must be decoupled.

IV. Observers Design

The competitiveness of markets and the need to reduce costs has led to a widespread tendency to search for new solutions. These solutions are often achieved by reducing the number of components or application of lighter and cheaper materials, among other methods. This also represents a challenge in terms of engineering, with demand for new and improved technical design, integration and control techniques. All these aspects have particular relevance for low power applications such as fractional horsepower motors and drives.

The proposed solution intends to be a simple, weightless and cheap solution using a unique current sensor in terms of measurement equipment. The applied armature voltage is obtained multiplying the known DC voltage by the switching states of power devices. Such states can be presumed from the previous gate signals (±*1*) assuming no failures in such power semiconductors.

Besides the previously measured motor parameters, no additional measurement devices are necessary to develop both speed and external torque observers. Other aspects, such as length of the wires, connectors, accuracy and nonlinearities of current sensors, etc., should also be considered during the design stage since they can influence the robustness and the global performance of the drive.

A. Speed and Torque Observers

According with control theory, a state observer is a structure that models a real system in order to provide an estimate of its internal state, given certain inputs and outputs measurements. The overall objective of the proposed state observers is estimating the speed and external torque known the motor parameters as well as the current and voltage input measured. Let be ξ the value to be observed and $\hat{\xi}$ the corresponding estimated value, as a result:

$$\hat{\xi} = \xi + \tilde{\xi} \tag{5}$$

where $\tilde{\xi}$ is the error of the estimated $\hat{\xi}$. The aim is to nullify $\tilde{\xi}$ and this can be attained with an appropriated first order differential equation:

$$\dot{\tilde{\xi}} = -g\tilde{\xi} \tag{6}$$

The solution of this equation is:

$$\tilde{\xi} = \tilde{\xi}_0 e^{-gt} \tag{7}$$

where $\tilde{\xi}_0$ is the initial error of $\tilde{\xi}$. This equation states that the estimated error tends to zero with a constant time, g^{-1}, ie, the estimated value asymptotically converge to the actual value. Let be:

$$\begin{cases} \hat{T} = T + \tilde{T} \\ \hat{\omega} = \omega + \tilde{\omega} \end{cases} \tag{8}$$

The derivative of (8) considering (6) can be expressed by

$$\begin{cases} \dot{\hat{T}} = \dot{T} - g_1\tilde{T} \\ \dot{\hat{\omega}} = \dot{\omega} - g_2\tilde{\omega} \end{cases} \tag{9}$$

Considering slow variations of torque T or $\left|\dot{T}\right| << \left|g_1 T\right|$ the derivative $\left|\dot{T}\right|$ can be neglected, resulting in (10).

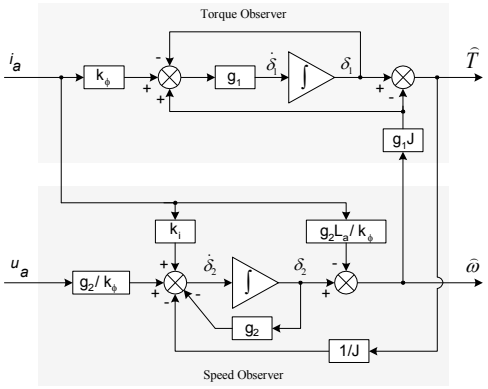

Fig. 4. Overall diagram proposed as speed and torque observers of a PMDC motor.

$$\begin{cases} \dot{\hat{T}} = -g_1\left(\hat{T} - \overbrace{k_\phi i_a + J\dot{\omega}}^{-T}\right) \\ \dot{\hat{\omega}} = \overbrace{\frac{k_\phi}{J} i_a - \frac{T}{J}}^{\dot{\omega}} - g_2\hat{\omega} + g_2 \overbrace{\frac{1}{k_\phi}\left(u_a - r_a i_a - L_a \dot{i}_a\right)}^{\omega} \end{cases} \tag{10}$$

Two dummy variable δ_1 and δ_2 (11) can be used to help construct the observer.

$$\begin{cases} \delta_1 = \hat{T} + g_1 J\omega \\ \delta_2 = \hat{\omega} + \frac{g_2}{k_\phi} L_a i_a \end{cases} \tag{11}$$

Using (11) into (10) and grouping the derivative terms:

$$\begin{cases} \dot{\delta}_1 = -g_1\left(\delta_1 - g_1 J\omega - k_\phi i_a\right) \\ \dot{\delta}_2 = -g_2\delta_2 + \underbrace{\left(\frac{g_2^2}{k_\phi} L_a + \frac{k_\phi}{J} - g_2\frac{r_a}{k_\phi}\right)}_{k_i} ia + \frac{g_2}{k_\phi} u_a - \frac{T}{J} \end{cases} \tag{12}$$

In this model, the voltage and current are measured. The speed and external torque are unknown but, instead, will use their estimated values ($\hat{T}$ and $\hat{\omega}$). The observer outputs are obtained using (12) and as can be seen in Fig. 4. The torque observer output ($\hat{T}$) is one input of the speed observer output ($\hat{\omega}$) and vice versa.

B. Observers Performance

As presented earlier, the observers were developed from a mathematical modeling based on a first order differential equation obtained from the motor state model. Because the observers structure depends on the motor parameters and measured values, their experimental determination will contain certainly errors, and the observers performance will be affected. Several simulations were made to evaluate those errors. The simulation tests were implemented in Matlab/Simulink software using the SimPowerSystem tool.

Fig. 5 shows the simulation of the speed observer errors produced due to variations in voltage and armature current,

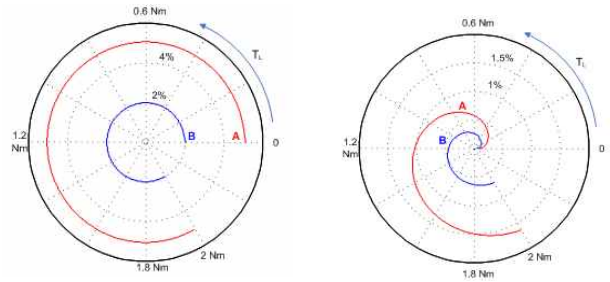

With U_a error With i_a error

Fig. 5. Speed error resulting from deviations of 5% (A) and 2% (B) of U_a and i_a with torque variation from no-load to full load (2Nm).

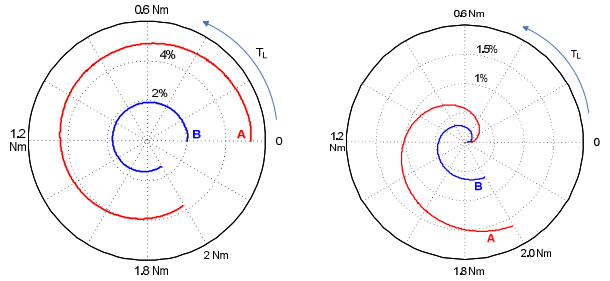

With k_ϕ error With r_a error

Fig. 6. Speed error resulting from deviations of 5% (A) and 2% (B) of k_ϕ and r_a with torque variation from no-load to full load (2Nm).

which can also be interpreted as measurement errors. The variation values used in the observer were 95% (A) and 98% (B) of the real ones. Also, the shaft torque increased from no-load to full load (2 Nm).

The voltage variations are reflected in the speed error proportionally to load variation. The experimental implementation must be carefully designed even using a constant power sources due to undesired drop voltages on connection wires or unexpected contact resistances. The effects of the current variations in the speed error are rather small compared with the voltage variations; however the accuracy of the current sensor should not be neglected.

Fig. 6 presents simulations of the speed observer errors due to the torque constant k_ϕ and resistance armature r_a variations.

The effect of k_ϕ variation in the speed error decreases lightly with the load torque condition but it is almost as important as the voltage variation. Obviously, its determination must be as rigorous as possible; one should take into account that armature reaction can produce an eventual local demagnetization of the permanent magnets and, as consequence, k_ϕ can vary between no-load and full load conditions. A model to obtain k_ϕ can be implemented considering its dependence of the armature current, but since k_ϕ variation is relatively small in fractional horsepower PMDC motors, it can be considered constant. In the presented work the k_ϕ variable was considered constant with amplitude corresponding to the no-load condition, close of the saturation state.

The armature resistance r_a variation, like the error of the measured current i_a, leads to higher errors for higher load torques, but, in both cases, even a 5 % variation does not overcome 2 % of the final speed error. Again the connection wires or unexpected contact resistances can lead to undesirable errors.

Additional simulations revealed that the inductance L_a and the inertia momentum J just influences the current and speed during transient responses.

C. Controller Limitation

The observer was designed considering slow torque variations. Nevertheless, the motor can present Coulomb friction and/or cogging torque. The first one has a mechanical nature and it is characterized by a discontinuous torque when the speed is reversed. The magnetic interaction between the magnet permanents and the slotted armature of the motor has an inconvenient cogging torque. If the rotor is turned slowly by hand is perceptible that there are attraction zones, followed by repulsion zones and neutral regions. Although the cogging torque average is zero and does not contribute to the rotation, their presence causes vibrations and speed ripple, particularly at light load and low speed conditions [28]. Since Coulomb friction and the cogging torque were not considered, the controller presents some limitations when crossing the zero speed slowly.

V. Stability Analysis

In this section a brief stability analysis using the classic approach is presented. Let us assume a continuous linear, time-invariant (LTI) system expressed in the state-space form as [29]:

$$G(s) = C(sI - A)^{-1}B + D = \frac{C[adj(sI - A)]B}{det(sI - A)} + D \qquad (13)$$

The physical stability of the LTI obtained from the state-space representation of a system is determined completely by the eigenvalues of matrix A, which are the roots of characteristic equation, *R(s):*

$$R(s) = det(sI - A) = 0 \qquad (14)$$

Based on equations (10)-(12) and according to principle of superposition, this LTI MIMO (Multiple-Input and Multiple-Output) system can be expressed by the following SISO (Single-Input and single-Output) transfer functions (15)-(16). A linear, time-invariant system is stable if the natural response approaches zero as time approaches infinity. This means that this system is stable if every bounded input yields a bounded output. In the S-domain, it is required that all the poles of the system are located in the left half-plane, and

therefore every solution is stable if all the eigenvalues of matrix A have negative real part.

$$\frac{\hat{\omega}}{u_a}=\frac{g_2}{k_\phi(s+g_2)};\ \frac{\hat{\omega}}{i_a}=\frac{-g_2L_as+k_\phi k_i}{k_\phi(s+g_2)};\ \frac{\hat{\omega}}{\hat{T}}=-\frac{g_1Js}{(s+g_1)} \tag{15}$$

$$\frac{\hat{T}}{i_a}=\frac{g_1k_\phi}{(s+g_1)};\quad \frac{\hat{T}}{\hat{\omega}}=-\frac{1}{J(s+g_2)} \tag{16}$$

According to stability criteria, system is asymptotically stable if ($g_1>0$) and ($g_2>0$). Since zeros of the transfer functions located in the left side of poles increase stability, reducing time response, this principle can be used to calculate g_2. Based on (15) g_2 must provide that $k_i < L_a/k_\phi$, and consequently:

$$g_2^2-g_2\frac{r_a}{L_a}+\left(\frac{k_\phi^{\ 2}}{L_aJ}-1\right)<0 \tag{17}$$

Since all transfer functions presented in (15)-(16) meet a transient response specification for systems of first order and considering that ($g_1>0$) and ($g_2>0$), the graphical representation of root locus is unnecessary to demonstrate asymptotic stability.

The selection and adjustment of parameters g1 and g2 can be accomplished with Nyquist stability criteria for frequency response. In the diagrams of Fig.7 can be seen the effect of variation of g1 and g2 in the S-domain for transfer functions presented in (15)-(16). To achieve stability according to Nyquist criteria the coordinate s = -1+j0 must be mapped outside of the closed region. The Nyquist diagrams demonstrate that only mechanical transfer functions (Fig. 7 a) and b)) can become unstable due to variation of parameters g1 and g2. The remaining transfer functions are not affected by these parameters (Fig. 7 c), d) and e)). Increasing g2 above certain values tends to avoid system instability to frequency response (Fig. 7 a)). On the contrary, increasing g1 outside certain limits tends to introduce instability to frequency response (Fig. 7 b)).

VI. HARDWARE IMPLEMENTATION

To perform the hardware implementation in laboratory, a controlled 30 V_{DC} voltage source was selected to supply a four-quadrant chopper and feed the PMDC motor. Alternatively, a battery or other regulated AC/DC converter could be used. The core of the controller is based on a dsPIC30F4011 device. This device is responsible for speed and external torque estimation according with the proposed observers, speed control through the sliding mode control technique, current limiter and PWM drive signal generator including dead-times. A small conditioning circuit was also developed to accommodate the measured current and speed reference signals to the dsPIC device.

Due to the sequential nature of programming such devices,

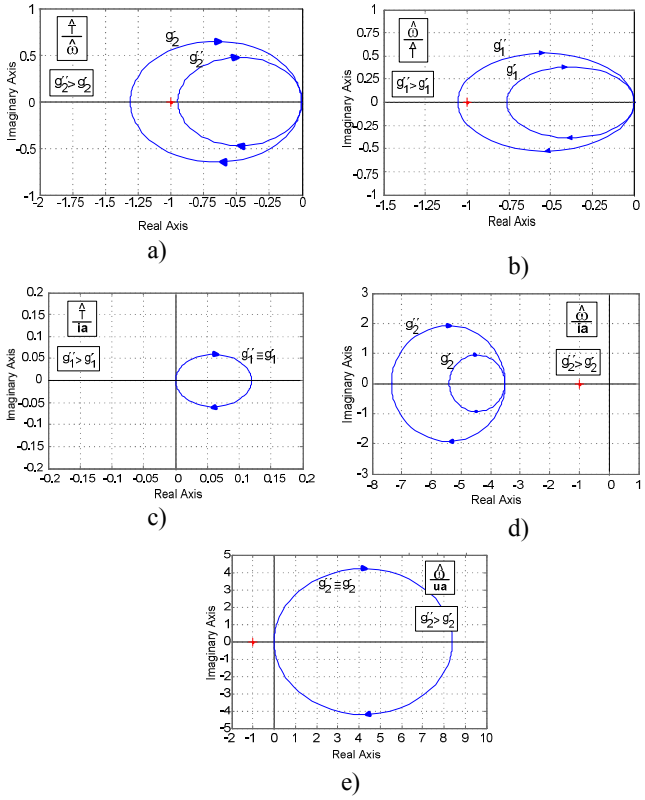

Fig. 7. Nyquist diagrams of transfer functions (15)-(16).

instead of using the switching function presented in (2) with derivative error, it was considered the difference between the speed error in two consecutive steps *j-1* and *j* (18).

$$S(\omega,t)=\left[(e_\omega)_j-(e_\omega)_{j-1}\right]+k_\omega(e_\omega)_j \tag{18}$$

Based on same principle, an additional acceleration observer (19) could also be added, leading to the estimated switching function (20). This approach was not explored in this paper. For slow variations of ω_{ref} it can be considered $\gamma_{ref}\cong 0$ or, alternatively, γ_{ref} can be obtained from ω_{ref}.

$$\hat{\gamma}=\frac{k_T\phi\, i_a}{J}-\frac{\hat{T}}{J} \tag{19}$$

$$\hat{S}=\gamma_{ref}-\frac{k_T\phi\, i_a}{J}-\frac{\hat{T}}{J}+k_\omega\left(\omega_{ref}-\hat{\omega}\right) \tag{20}$$

The overall hardware implementation to the sensorless speed control of a PMDC motor can be seen in Fig. 8.

The system is composed by the power source, DC/DC converter, current sensor, conditioning circuit, dsPIC device and PMDC motor. In this work, the estimated torque $\hat{T}$ was only used to obtain an estimate of speed; however, it is readily accessible for its measurement or even to satisfy other control objectives. Although a voltage sensor could be included, in low power drives, it is advisable and desirable to use a low cost

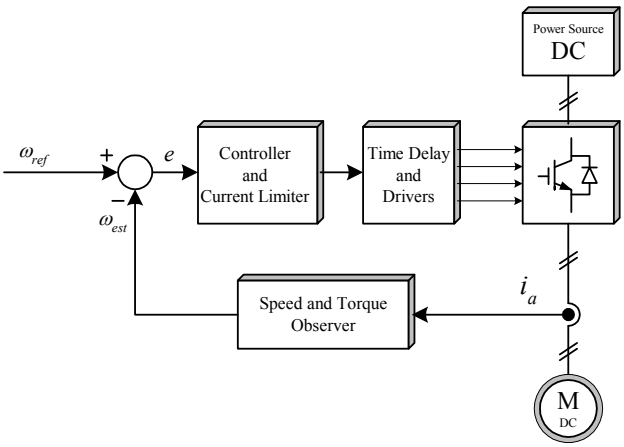

Fig. 8. Overall proposed hardware solution.

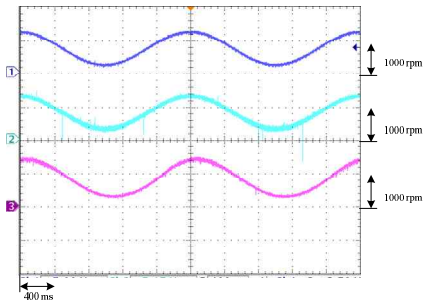

Fig. 9. Drive performance test obtained with a sinusoidal reference signal of amplitude peak to peak about 1000 rpm at no-load condition. From top to bottom, the curves represent the reference, the estimated and the real speed.

solution and so the armature voltage was calculated in the dsPIC device according with (21). The source voltage U_{dc} and the connection resistance R_C must be previously measured to avoid undesirable error as seen before.

$$u_a = \text{sgn\_}U_a \cdot \left(U_{dc} - R_C \cdot i_a\right) \tag{21}$$

VII. EXPERIMENTAL RESULTS

In this section some experimental results of the proposed control solution are presented. The experimental result of the drive performance to a sinusoidal speed reference is shown in Fig. 9. The first curve is a sinusoidal reference signal obtained from a function generator with frequency around 0.5 Hz, and equivalent speed from 300 rpm to 1300 rpm. The middle curve is the estimated observer speed obtained from the digital PWM output of the dsPIC device and combined with a low-pass filter. The last curve is the real speed measured with a DC tachymeter to compare the results. In this case, there is a good correspondence between the reference, the estimated and the real speed despite a short time delay. The presented results were obtained at no-load condition. Same experimental test in full load condition revealed very similar results.

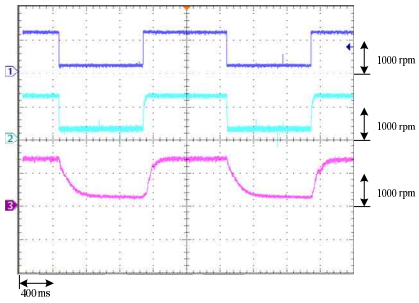

Fig. 10. Drive performance test obtained with a square reference signal of amplitude peak to peak about 1000 rpm at full load condition. From top to bottom, the curves represent the reference, the estimated and the measured speed.

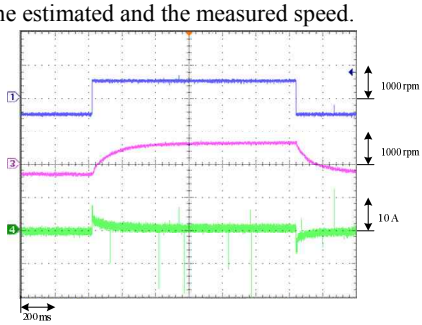

Fig. 11. Drive performance test to current limiter during speed reversal. From top to bottom, the curves represent the reference speed, the measured speed and the armature current.

The drive was also tested with square reference signals as can seen in Fig.10. Previous specifications (0.5 Hz, lowest speed of 300 rpm and highest speed of 1300 rpm) are valid but in this case the experimental tests were performed at full load condition. In this case is also evident the small time delay between reference and real speed. This delay can be explained by assumptions made considering slow variations of torque T in the observers design as well as other considerations (see section IV.C). Also delays in digital signal processing are responsible for this situation. The results can be considered very satisfactory regardless of these delays.

The performance of the current limiter was also analyzed. Fig. 11 shows the reference and real speed (from -600 rpm to 600 rpm) and the armature current. It can be seen the current limitation provided by the drive. More details about the current limiter actuation can be observed in Fig. 12, where current oscillates around I_{max} during some milliseconds due to rotor speed reversal.

The behavior of the drive to external disturbances was also tested. Fig. 13 shows the introduction of an external torque disturbance after an increased step reference signal (200 rpm to 1400 rpm). This and other load tests were performed by a generator coupled to the PMDC motor. It can be observed that the real speed suffers a small reduction and thereafter recovers the initial value, eliminating the speed error. The current also increases, allowing the motor developing the adequate electromagnetic torque to drive the load.

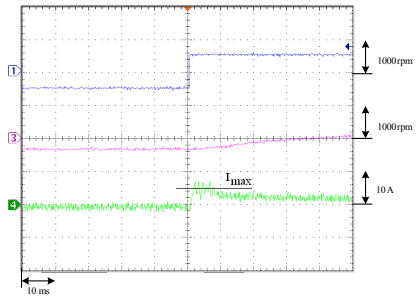

Fig. 12. Details of armature current limitation operating in different quadrants. From top to bottom, the curves represent the reference speed, the measured speed and the armature current.

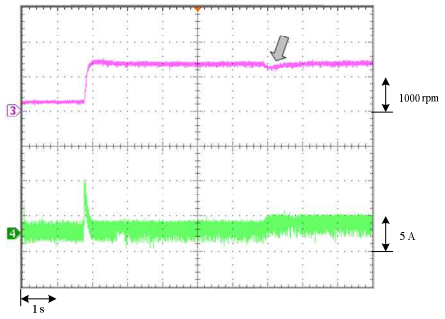

Fig. 13. Experimental drive test to external torque disturbances. From top to bottom, the curves represent the measured speed and the armature current.

VIII. Conclusions

A sensorless PMDC motor speed controller for low power applications was presented and its effectiveness and robustness was analyzed by several experimental results. The proposed solution can be easily adapted to speed or torque control.

The experimental results to speed control revealed that the rotor speed reaches and tracks the speed reference without relevant damping or overshoot in several load conditions, confirming the performance characteristics of the sliding mode control. Some delays in the real speed were detected due to some simplifications in the observers design, although without compromise the main control objective.

The control decision is based on a simple switching function which allows to nullify the tracking error according with the sliding mode control strategy proposed. A protective current limiter was successfully integrated in the controller using simple logic functions. This approach increases the overall level of safety.

It was also objective of this work present some contributions to the creation of low-cost control solutions, and so, speed and external torque observers were developed based only on motor parameters, armature current measurement and voltage presumed from switching state of power devices.

Appendix

The following are presented motor characteristics:

Power	P [W]	400
Armature Voltage	U [V]	24
Armature Resistance	$R_a[\Omega]$	0.43
Armature Inductance	L_a [mH]	0.795
EMF constant	K_ϕ [Vs/rad]	0.119
Speed	N [rpm]	2000
Moment of Inertia	J [kgm^2]	0.659
Viscous Friction	k_D [Nms]	0.0002
Coulomb Friction	k_C [Nm]	0.0951

References

[1] S. Ye and K. T. Chau, "Chaoization of DC motors for industrial mixing," *IEEE Trans. Ind. Electron*., Vol. 54, No 4, pp. 2024-2032, Aug. 2007.

[2] J. L. Flores, H. S. Ramirez, E. F. C. Lopez, and M. A. C. Ordaz, "Sensorless passivity based control of a DC motor via a solar powered sepic converter-full bridge combination," *Journal of Power Electronics*, Vol. 11, No. 5, pp. 743-750 , Sep. 2011.

[3] C. C. Tsai, H.-C. Huang, and S. C. Lin, "Adaptive neural network control of a self-balancing two-wheeled scooter," *IEEE Trans. Ind. Electron*., Vol. 57, No. 4, pp. 1420-1428, Apr. 2010.

[4] R. Kahoul, Y. Azzouz, P. Marchal, and B. Mazari, "New behavioral modeling for DC motor armatures applied to automotive EMC characterization," *IEEE Trans. Electromagn. Compat.*, Vol. 52, No 4, pp. 888-901, Nov. 2010.

[5] R. Letor, A. Tesla, and S. Di Caro, "Estimation of the shaft position on low-cost DC actuators," in *Proc. ISIE,* pp. 440-445, Jul. 2010.

[6] A. Consoli, G. Bottiglieri, R. Letor, R. Ruggeri, A. Testa, and S. De Caro, "Sensorless position control of DC actuators for automotive applications," *IEEE- 39th Annual Meeting Industry Applications Conference*, Vol. 2, pp. 1217-1224, Oct. 2004.

[7] J. Scott; J. McLeish, and W. H. Round, "Speed control with low armature loss for very small sensorless brushed DC motors," *IEEE Trans. Ind. Electron*., Vol. 56, No 4, pp. 1223-1229, Apr. 2009.

[8] J. G. Llorente, E. I. O. Rivera, A. S. Llinas, and E. J. Brea, "Analyzing the optimal matching of DC motors to photovoltaic modules via DC-DC converters," *IEEE 25th in Proc. APEC*, pp. 1062-1068, Feb. 2010.

[9] T. Castagnet and J. Nicolai, "Digital control for brush DC motor," *IEEE Trans. Ind. Appl.*, Vol. 30, No. 4, pp. 883-888, Jul./Aug. 1994.

[10] J. L. Flores, J. Reger, and H. S. Ramírez, "Load torque estimation and passivity-based control of a boost-converter/DC-motor combination," *IEEE Trans. Contr. Syst. Technol.*, Vol. 18, No. 6, pp. 1398-1405, Nov. 2010.

[11] G. Mirzaeva, R. E. Betz, and T. J. Summers, "Evaluation of current density in DC motor brushes for mining machines based on air-gap field measurement," *IEEE Trans. Ind. Appl.*, Vol. 46, No. 4, pp. 1255-1263, Jul./Aug. 2010.

[12] S. I. Amer and M. M. Salem, "A comparison of different

intelligent control techniques for a PM DC motor," *Journal Power Electronics*, Vol. 5, No. 1, pp. 1-10, Jan. 2005.
[13] C.-L. Hwang, L.-J. Chang, and Y.-S. Yu, "Network-based fuzzy decentralized sliding-mode control for car-like mobile robots," *IEEE Trans. Ind. Electron*., Vol. 54, No. 1, pp. 574–585, Feb. 2007.
[14] J. O. Jang, "Neural network saturation compensation for DC motor systems," *IEEE Trans. Ind. Electron*., Vol.54, No.3, pp. 1763-1767 Jun. 2007.
[15] G. G. Rigatos, "Adaptive fuzzy control of DC motors using state and output feedback: Application to DC Motors of robotics Manipulators," *Proc. International Symposium on Advanced Intelligent Systems, ISIS*, pp. 1-6, 2007.
[16] D. Kukolj, F. Kulic, and E. Levi, "Design of the speed controller for sensorless electric drives based on AI techniques: a comparative study," *Artificial Intelligence in Engineering - Elsevier*, Vol. 14, pp. 165-174, May 2000.
[17] S K. Narebda, "Neural networks for control: theory and practice," in *Proc IEEE*, Vol. 84, No 10, pp. 1385-1406, Oct. 1996.
[18] H. Butler, G. Honderd, and J. van Amerongen, "Model reference adaptive control of a direct drive DC motor," *IEEE Control Syst. Mag.*, Vol. 9, No. 1, pp. 80-84, Jan. 1989.
[19] S. F. Alyaqout, P. Y. Papalambros and A. G. Ulsoy, "Combined robust design and robust control of an electric DC motor," *IEEE/ASME IEEE Trans. Mechatronics*, Vol. 16, No. 3, pp. 574-582, Jun. 2011.
[20] C. Attaianese, A. Perfetto, G. Tomasso, "Robust position control of DC drives by means of H∞ controllers," *in Proc. Inst. Elect. Eng.-Elect. Power Appl.*, Vol. 146, No. 4, pp. 391-396, Jul. 1999.
[21] J. L. Flores, J. Reger, H. S. Ramirez, "Speed-sensorless tracking control of a DC-motor via a double Buck-converter," *45th IEEE Conference on Decision and Control*, pp. 6229-6234, Dec. 2006.
[22] P. Chevrel and S. Siala, "Robust DC-motor speed control without any mechanical sensor," in *Proc. IEEE Int. Conf. Control Appl.*, pp. 244-246, Oct. 1997.
[23] G. S. Buja, R. Menis, and M. I. Valla, "disturbance torque estimation in a sensorless DC drive," *IEEE Trans. Ind. Electron*., Vol. 42, No. 4, pp. 351-357, Aug. 1995.
[24] A. Pisano, A. Davila, L. Fridman, and E. Usai, "Cascade control of PM DC drives via second-order sliding-mode technique," *IEEE Trans. Ind. Electron*., Vol. 55, No. 11, pp. 3846-3854, Nov. 2008.
[25] A.-M. M. A. Mohamed, "Sliding mode control design and application to permanent magnet DC motor speed control," *MEPCON'2006 - The Eleventh International Middle East Power Systems Conference*, pp. 25-29, Sep. 2006**.**
[26] J. E. Slotine and W. Li, *Applied Nonlinear Control I*, Prentice Hall, 1991.
[27] V. Utkin, J. Guldner, and J. Shi, *Sliding Mode Control in Electromechanical Systems*, Taylor & Francis, 1999.
[28] Z. Q. Zhu, "A simple method for measuring cogging torque in permanent magnetic machines," *PES'2009 – IEEE Power & Energy Society General Meeting*, 2009.
[29] J. H. Taylor and C. Chan, "Matlab Tools for linear and nonlinear systems stability theorem implementation," in *Proc. IEEE Conference on Control Applications*, USA, 1997.

M. G. Guerreiro was born in S.Teotónio, Portugal, on 1951. He received the Dipl. Ing., the M.S. and Ph.D. degrees in electrical engineering from Instituto Superior Técnico, Technical University of Lisbon, Lisbon, Portugal in 1975, 1992 and 2000, respectively. Since 1990, he has been with the Polytechnic Institute of Setúbal, Superior Technical School of Setúbal, where he teaches Electrical Machines as Adjoint Professor of the Electrical Engineering Department. His research interests include electrical machines, variable-speed drives, renewable energy generation, modeling and simulation.

D. Foito was born in Portugal, on January 21, 1968. He received the Dipl. Ing. and M.S. degrees in electrical engineering from Instituto Superior Técnico, Technical University of Lisbon, Lisbon, Portugal in 1993 and 2002, respectively. Since 1997 he is a member of the teaching staff at Electrical Engineering Department of Superior Technical School of Setúbal – Polytechnic Institute of Setúbal. Presently he is a Adjoint Professor, teaching Power Electronics and Electric Drives. His research interests include renewable energy generation, electrical machines, electric drives and electric vehicle.

A. Cordeiro was born in Portugal, on March 29, 1976. He received the B.S. degree in Electrical Engineering from Institute Superior of Engineering of Lisbon, Portugal, in 1999 and the M.S. Degree in Electrical and Computer Engineering from Technical University of Lisbon, Portugal, in 2004. Member of the teaching staff at Electrical Engineering Department of Superior Technical School of Setúbal between 1999 and 2006 – Polytechnic Institute of Setúbal. Member of the teaching staff at Electrical Engineering and Automation Department, Institute Superior of Engineering of Lisbon – Polytechnic Institute of Lisbon since April 2006, he is a Professor, teaching Automation and Robotics.